Inverse scattering for the homogeneous dispersive anisotropic slab using transient electromagnetic fields

Friden, Jonas

1994

CODEN:LUTEDX/(TEAT-7031)/1-24/(1994)
Revision No. 1: August 1995

Inverse scattering for the homogeneous dispersive anisotropic slab using transient electromagnetic fields

Jonas Fridén

Electromagnetic Theory
Department of Electrical and Information Technology
Lund University
Sweden

Jonas Fridén

Institute of Theoretical Physics
Chalmers University of Technology
University of Göteborg
SE-412 96 Göteborg
Sweden

Editor: Gerhard Kristensson

Abstract

An inverse scattering problem for a slab containing a homogeneous dispersive anisotropic medium is investigated. The inverse problem is to recover two three-dimensional dyadic susceptibility kernels from knowledge of the scattering kernels. Time domain techniques involving transient electromagnetic plane waves, wave splitting, invariant imbedding and a Green function technique are used. The inverse problem is separated into two parts: The Dynamics Inverse Problem (DIP) and Retrieval of Interior Parameters (RIP). Furthermore, mirror images and the Mirror Image Pair (MIP) are discussed. The DIP is solved numerically by using an inverse algorithm and scattering data from one MIP. The RIP turns out to be well posed (system of Volterra equations of the second kind) and needs in general two MIPs. In the DIP, the equations for initial values using transmission data have in general not a unique solution. Constraints and simplifications for certain classes of media are pointed out. Numerical examples, including noisy data, illustrate the analysis.

1 Introduction

An inverse scattering problem using transient electromagnetic plane waves is investigated. The scatterer is a slab containing a homogeneous, dispersive and anisotropic medium. This is a relevant study for the non-destructive testing of thin anisotropic layers such as liquid crystals or the design of artificial media for microwave applications, e.g. coatings with prescribed scattering properties. The analysis can easily be converted for use in anisotropic layers where the anisotropy is induced by an external static field, i.e., gyrotropic media with Faraday or Kerr effect.

The main objective of this paper (the inverse problem) is to recover two three-dimensional susceptibility dyadics $\boldsymbol{\chi}_e$ and $\boldsymbol{\chi}_m$ from scattering data generated by obliquely incident transient plane waves. In this context, the questions of which experiment and scattering data to use, naturally arise. More precisely:

(i) Which plane waves are needed?

(ii) Should one use transmission- and/or reflection-data?

The basic tools for the inverse problem have been developed in Refs [4, 5] for wave propagation in anisotropic media. Here, these tools are slightly generalized, see below. Closely related direct and inverse problems for dispersive media [1, 10, 11, 14] and non-dispersive anisotropic media [15] have also been solved using similar techniques. A wave splitting technique [2, 16] is used together with both an invariant imbedding approach [1] and a Green functions technique [9]. The wave splitting technique leads to an equation for the split electromagnetic fields. This equation is equivalent to the Maxwell equations and it describes the dynamics of right- and left-going electromagnetic waves. In this context the medium is represented by four two-dimensional dyadics ($\boldsymbol{\Delta}_{kl}$-dyadics).

In Ref. [4] mirror images are investigated. Here, the mirror image concept is used to full extent, i.e., the basic tools are generalized using mirror images. The

equations for the mirror image scattering experiments comprise the complete set of scattering data needed for the inverse problem. This set is generated by a pair of scattering experiments with mirror image incident waves, see Section 3, denoted MIP (Mirror Image Pair).

It is natural to solve the inverse problem in two parts:

(I): The DIP (Dynamics Inverse Problem) is to reconstruct $\boldsymbol{\Delta}_{kl}$ (the representation of the medium in the dynamics for the split fields) from scattering data. The scattering data needed here is the complete set of scattering data generated by a MIP.

(II): The RIP (Retrieval of Interior Parameters) is to retrieve the susceptibility dyadics $\boldsymbol{\chi}_e$ and $\boldsymbol{\chi}_m$ from the $\boldsymbol{\Delta}_{kl}$-dyadics.

Solving the DIP is the hard problem and there is no proof, so far, on well-posedness. On the other hand under certain conditions on the MIP (or MIPs) the RIP is a well-posed problem with a unique solution. Therefore, by separating the inverse problem in the DIP and the RIP, the possible ill-posedness is moved to the DIP. Furthermore, the investigation of the RIP gives the answer to question (*i*) and the DIP to question (*ii*), see Sections 4.1 and 4.2, respectively.

To solve for the initial values in the DIP using transmission data, i.e., wave front propagators and transmission kernels at zero time, some restrictions have to be made. Physically, the wave front propagators may comprise oscillating parts, and part of the inverse problem (the DIP) would be to tell the number of these oscillations from knowledge of the initial and final states of the wave front. Even worse, for some directions of incidence, crucial information about the complexity of the medium is completely washed out. The relevant equations turn out to have either a non-unique or no solution at all. For some media this can be the case for all directions of incidence and for other media certain sectors of the incident direction have this property. The remedy for this problem is to use a slab that is so thin that only less than one oscillation can take place. Fortunately, for reciprocal anisotropic media these equations always have a unique solution.

Note that in the derivation of the basic equations the medium is assumed to be continuously stratified. However, for the inverse problem the medium is assumed to be homogeneous.

2 Basic equations and wave splitting

The basic equations have been derived in earlier publications, see Refs [4, 5]. In this section these equations are reviewed in a dyadic setting and for general anisotropic media.

The combined Maxwell equations and constitutive relations [8] are[1]

$$\begin{cases} \nabla \times \boldsymbol{E}(\boldsymbol{r},t) = -\partial_t \mu_0 \left(\boldsymbol{H}(\boldsymbol{r},t) + \boldsymbol{\chi}_m(\boldsymbol{r},\cdot) * \boldsymbol{H}(\boldsymbol{r},\cdot)(t) \right), \\ \nabla \times \boldsymbol{H}(\boldsymbol{r},t) = \partial_t \epsilon_0 \left(\boldsymbol{E}(\boldsymbol{r},t) + \boldsymbol{\chi}_e(\boldsymbol{r},\cdot) * \boldsymbol{E}(\boldsymbol{r},\cdot)(t) \right). \end{cases}$$

[1]The symbol $*$ is a short hand notation for causal time convolution.

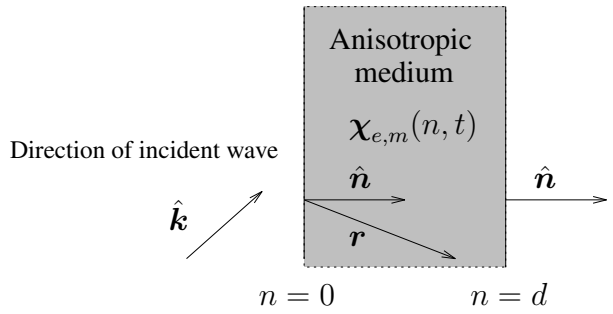

Figure 1: The geometry of the scattering experiment.

Here the susceptibility kernels $\boldsymbol{\chi}_e$ and $\boldsymbol{\chi}_m$ are three-dimensional dyadics that characterize the medium.

A transient plane wave impinges obliquely (along $\hat{\boldsymbol{k}}$) on a slab of thickness d containing the stratified anisotropic medium (normal $\hat{\boldsymbol{n}}$), see Fig. 1. The depth in the slab is given by the coordinate $n = \boldsymbol{r} \cdot \hat{\boldsymbol{n}} \in [0, d]$.

The explicit space and time dependence of the incident wave implies that the electromagnetic fields vary only with $n = \boldsymbol{r}\cdot\hat{\boldsymbol{n}}$ and $s = t - \boldsymbol{r}\cdot\boldsymbol{k}_\parallel/c_0$, cf. [5]. Therefore, the nabla operator becomes $\nabla = -(\boldsymbol{k}_\parallel/c_0)\partial_s + \hat{\boldsymbol{n}}\partial_n$. Vectors ($\boldsymbol{F} = \boldsymbol{E}, \boldsymbol{H}, \hat{\boldsymbol{k}}$) and dyadics are decomposed in normal and parallel components with respect to $\hat{\boldsymbol{n}}$, see [4]. The following notation is used:

$$\begin{aligned}
&\boldsymbol{F} = \boldsymbol{F}_\parallel + F_n\hat{\boldsymbol{n}},\\
&\boldsymbol{\chi}_\kappa = \boldsymbol{\chi}_{\parallel,\kappa} + \hat{\boldsymbol{n}}\boldsymbol{a}_\kappa + \boldsymbol{b}_\kappa\hat{\boldsymbol{n}} + \hat{\boldsymbol{n}}c_\kappa\hat{\boldsymbol{n}} \qquad \kappa = e, m.
\end{aligned}$$

The parallel and normal components of vectors and dyadics are obtained via the decomposition $\mathbf{I} = \mathbf{I}_\parallel + \hat{\boldsymbol{n}}\hat{\boldsymbol{n}}$ of the three-dimensional unit dyadic $\mathbf{I}$. Here, $\mathbf{I}_\parallel$ is the two-dimensional unit dyadic normal to $\hat{\boldsymbol{n}}$, i.e., $\hat{\boldsymbol{n}} \cdot \mathbf{I}_\parallel = \mathbf{I}_\parallel \cdot \hat{\boldsymbol{n}} = 0$. Parallel and normal components of the susceptibility dyadics are defined as

$$\begin{aligned}
\boldsymbol{\chi}_{\parallel,\kappa} &= \mathbf{I}_\parallel \cdot \boldsymbol{\chi}_\kappa \cdot \mathbf{I}_\parallel, \qquad \boldsymbol{a}_\kappa = \hat{\boldsymbol{n}} \cdot \boldsymbol{\chi}_\kappa \cdot \mathbf{I}_\parallel,\\
\boldsymbol{b}_\kappa &= \mathbf{I}_\parallel \cdot \boldsymbol{\chi}_\kappa \cdot \hat{\boldsymbol{n}}, \qquad c_\kappa = \hat{\boldsymbol{n}} \cdot \boldsymbol{\chi}_\kappa \cdot \hat{\boldsymbol{n}}.
\end{aligned}$$

Note, from this point on all vectors and dyadics are two-dimensional and normal[2] to $\hat{\boldsymbol{n}}$. The resolvent equations

$$c_\kappa + L_\kappa + c_\kappa * L_\kappa = 0 \qquad \kappa = e, m, \tag{2.1}$$

are used to eliminate the normal components of the fields, E_n and H_n.

A wave splitting transformation

$$\begin{aligned}
\begin{pmatrix} \boldsymbol{E}^+ \\ \boldsymbol{E}^- \end{pmatrix} &= \frac{1}{2}\begin{pmatrix} \mathbf{S}^{-1} & -\frac{1}{|k_n|}\mathbf{S} \\ \mathbf{S}^{-1} & \frac{1}{|k_n|}\mathbf{S} \end{pmatrix}\begin{pmatrix} \boldsymbol{E}_\parallel \\ \hat{\boldsymbol{n}} \times \eta_0\boldsymbol{H}_\parallel \end{pmatrix},\\
\mathbf{S}^{\pm 1} &= [(\hat{\boldsymbol{n}} \times \boldsymbol{k}_\parallel)(\hat{\boldsymbol{n}} \times \boldsymbol{k}_\parallel) + |k_n|^{\pm 1}\boldsymbol{k}_\parallel\boldsymbol{k}_\parallel]/(\boldsymbol{k}_\parallel \cdot \boldsymbol{k}_\parallel),
\end{aligned}$$

[2]This means $\mathbf{D} \cdot \hat{\boldsymbol{n}} = \hat{\boldsymbol{n}} \cdot \mathbf{D} = \mathbf{0}$ for any dyadic $\mathbf{D}$ and $\hat{\boldsymbol{n}} \cdot \boldsymbol{a} = 0$ for any vector $\boldsymbol{a}$, see [12].

is then applied to the equations for the parallel field components $\boldsymbol{E}_\parallel$ and $\boldsymbol{H}_\parallel$. The equation for the split fields $\boldsymbol{E}^\pm$ reads

$$v\partial_n \begin{pmatrix} \boldsymbol{E}^+ \\ \boldsymbol{E}^- \end{pmatrix} = \left[\begin{pmatrix} -\mathbf{I}_\parallel & 0 \\ 0 & \mathbf{I}_\parallel \end{pmatrix} + \begin{pmatrix} \boldsymbol{\Delta}_{11} & \boldsymbol{\Delta}_{12} \\ \boldsymbol{\Delta}_{21} & \boldsymbol{\Delta}_{22} \end{pmatrix} * \right] \partial_s \begin{pmatrix} \boldsymbol{E}^+ \\ \boldsymbol{E}^- \end{pmatrix}, \tag{2.2}$$

where $v = \frac{c_0}{|k_n|}$ is the phase velocity along $\hat{\boldsymbol{n}}$. The $\boldsymbol{\Delta}_{kl}$ dyadics are given by

$$\begin{pmatrix} \boldsymbol{\Delta}_{11} \\ -\boldsymbol{\Delta}_{12} \\ \boldsymbol{\Delta}_{21} \\ \boldsymbol{\Delta}_{22} \end{pmatrix} = \frac{1}{|k_n|} \mathcal{U} \begin{pmatrix} \frac{1}{|k_n|} \mathbf{S}\, \mathbf{D}_{me}\, \mathbf{S} \\ \mathbf{S}^{-1} \mathbf{D}_{ee} \mathbf{S} \\ \mathbf{S}\, \mathbf{D}_{mm} \mathbf{S}^{-1} \\ -|k_n| \mathbf{S}^{-1} \mathbf{D}_{em} \mathbf{S}^{-1} \end{pmatrix} \tag{2.3}$$

and the 4×4 matrix $\mathcal{U}$ is

$$\mathcal{U} = \mathcal{U}^{-1} = \frac{1}{2} \begin{pmatrix} -1 & 1 & 1 & 1 \\ 1 & -1 & 1 & 1 \\ 1 & 1 & -1 & 1 \\ 1 & 1 & 1 & -1 \end{pmatrix}.$$

Furthermore

$$\begin{aligned} \mathbf{D}_{me} &= \boldsymbol{\chi}_{\parallel,e} - \boldsymbol{b}_e * (1 + L_e *) \boldsymbol{a}_e - (\hat{\boldsymbol{n}} \times \boldsymbol{k}_\parallel)(\hat{\boldsymbol{n}} \times \boldsymbol{k}_\parallel) L_m, \\ \mathbf{D}_{ee} &= (1 + L_e *) \boldsymbol{k}_\parallel \boldsymbol{a}_e + (1 + L_m *)(\hat{\boldsymbol{n}} \times \boldsymbol{b}_m)(\hat{\boldsymbol{n}} \times \boldsymbol{k}_\parallel), \\ \mathbf{D}_{mm} &= (1 + *L_e) \boldsymbol{b}_e \boldsymbol{k}_\parallel + (1 + *L_m)(\hat{\boldsymbol{n}} \times \boldsymbol{k}_\parallel)(\hat{\boldsymbol{n}} \times \boldsymbol{a}_m), \\ \mathbf{D}_{em} &= -\boldsymbol{k}_\parallel \boldsymbol{k}_\parallel L_e - \hat{\boldsymbol{n}} \times \boldsymbol{\chi}_{\parallel,m} \times \hat{\boldsymbol{n}} - (\hat{\boldsymbol{n}} \times \boldsymbol{b}_m) * (1 + L_m *)(\hat{\boldsymbol{n}} \times \boldsymbol{a}_m). \end{aligned} \tag{2.4}$$

Note, each set of $\boldsymbol{\Delta}_{kl}$-dyadics is uniquely determined by $\boldsymbol{k}_\parallel$, $\boldsymbol{\chi}_e$ and $\boldsymbol{\chi}_m$.

3 Scattering kernels

In order to solve the direct and the inverse scattering problems, the scattering kernels are introduced. These kernels map the incident field to the scattered reflected and transmitted fields. Furthermore, the equations for the scattering kernels connect the $\boldsymbol{\Delta}_{kl}$-dyadics in the dynamics (2.2) to the scattering kernels. In Ref. [5] these equations are derived for an incident direction $\hat{\boldsymbol{k}}$ by using an imbedding or a Green functions method. To solve the inverse problem of reconstructing four (formally independent) $\boldsymbol{\Delta}_{kl}$-dyadics from scattering data, these methods have to be slightly generalized. Two directions of incidence are needed, namely $\hat{\boldsymbol{k}}^\pm = \boldsymbol{k}_\parallel \pm k_n \hat{\boldsymbol{n}}$ with corresponding incident fields $\boldsymbol{E}^\pm$. Note that both directions $\hat{\boldsymbol{k}}^\pm$ correspond to the same $\boldsymbol{\Delta}_{kl}$-dyadics since $\mathbf{I}_\parallel \cdot \hat{\boldsymbol{k}}^\pm = \boldsymbol{k}_\parallel$. A pair $\hat{\boldsymbol{k}}^\pm$ of incident directions, see Fig. 2, is denoted Mirror Image Pair (MIP) in the following. In a physical experiment two polarizations have to be considered for each incident direction, i.e., four polarizations for a MIP. The scattering kernels defined in this section comprise the scattering data of all possible polarizations and to stress the important quantity ($\boldsymbol{k}_\parallel$) for the inverse problem the MIP is used.

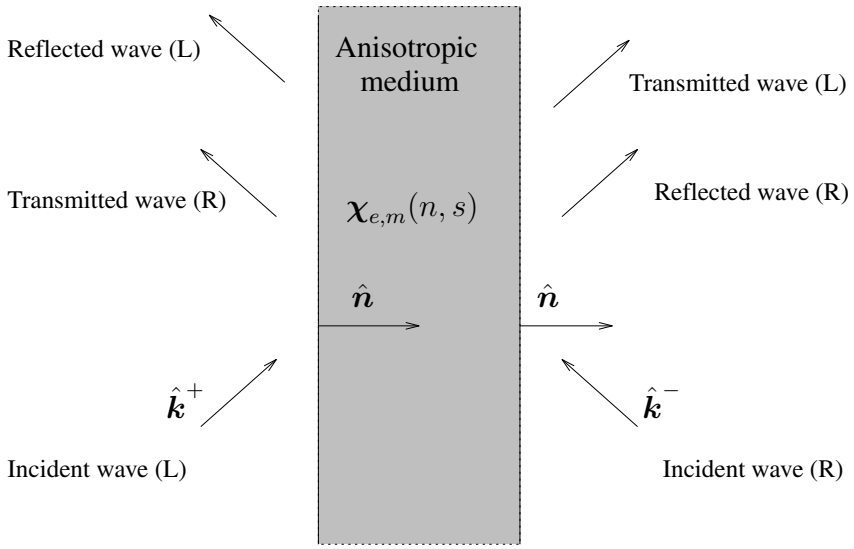

Figure 2: The incident and scattered waves of an L/R MIPE. The L/R index denotes an incoming wave from the left/right, respectively.

Below, the slightly generalized imbedding and Green functions equations for a MIP are presented. The scattering kernels are labeled with an index L or R referring to an incoming field from the left or the right, respectively.

In the imbedding method the L-case kernels $\mathbf{R}_L(n,s)$ and $\mathbf{T}_L(n,s)$ correspond to reflection and transmission due to the subslab $[n,d]$ and for the R-case kernels the subslab is $[0,n]$, cf. [5].

$$\begin{aligned}
\boldsymbol{E}^-(n,s) &= \mathbf{R}_L(n,\cdot) * \boldsymbol{E}^+(n,\cdot)(s),\\
\boldsymbol{E}^+(d,s+(d-n)/v) &= \mathbf{Q}^+(n,d)\left\{\boldsymbol{E}^+(n,s) + \mathbf{T}_L(n,\cdot) * \boldsymbol{E}^+(n,\cdot)(s)\right\},\\
\boldsymbol{E}^+(n,s) &= \mathbf{R}_R(n,\cdot) * \boldsymbol{E}^-(n,\cdot)(s),\\
\boldsymbol{E}^-(0,s+n/v) &= \mathbf{Q}^-(n,0)\left\{\boldsymbol{E}^-(n,s) + \mathbf{T}_R(n,\cdot) * \boldsymbol{E}^-(n,\cdot)(s)\right\}.
\end{aligned}$$

The Green functions $\mathbf{G}^{\pm}_{L/R}$ map an incident field from the left/right to the split field component $\boldsymbol{E}^{\pm}(n,s)$ in the slab, cf. [5]. In this method the kernels refer to the physical slab $[0,d]$. The definitions are

$$\begin{aligned}
\boldsymbol{E}^+(n,s+n/v) &= \mathbf{Q}^+(0,n)\boldsymbol{E}^+(0,s) + \mathbf{G}^+_L(n,\cdot) * \mathbf{Q}^+(0,n)\boldsymbol{E}^+(0,\cdot)(s),\\
\boldsymbol{E}^-(n,s+n/v) &= \mathbf{G}^-_L(n,\cdot) * \mathbf{Q}^+(0,n)\boldsymbol{E}^+(0,\cdot)(s),\\
\boldsymbol{E}^+(n,s+(d-n)/v) &= \mathbf{G}^+_R(n,\cdot) * \mathbf{Q}^-(d,n)\boldsymbol{E}^-(d,\cdot)(s),\\
\boldsymbol{E}^-(n,s+(d-n)/v) &= \mathbf{Q}^-(d,n)\boldsymbol{E}^-(d,s) + \mathbf{G}^-_R(n,\cdot) * \mathbf{Q}^-(d,n)\boldsymbol{E}^-(d,\cdot)(s).
\end{aligned}$$

The dyadics $\mathbf{Q}^{\pm}(n_1,n_2)$ propagate finite jump discontinuities (wave fronts) in the fields $\boldsymbol{E}^{\pm}$, respectively, from n_1 to n_2 along the characteristics of Eq. (2.2), cf. [5].

For homogeneous media $\mathbf{Q}^{\pm}(n_1,n_2)=\exp(-\boldsymbol{a}^{\pm}(n_2-n_1))$ where $\boldsymbol{a}^{+}=-\boldsymbol{\Delta}_{11}(0^{+})/v$ and $\boldsymbol{a}^{-}=-\boldsymbol{\Delta}_{22}(0^{+})/v$. Combined use of the above definitions and the dynamics (2.2) yields, see [5], the imbedding equations

$$\begin{aligned}
(v\partial_n-2\partial_s)\mathbf{R}_L &= \partial_s\boldsymbol{\Delta}_{21}+\partial_s\left\{\boldsymbol{\Delta}_{22}*\mathbf{R}_L-\mathbf{R}_L*\boldsymbol{\Delta}_{11}-\mathbf{R}_L*\boldsymbol{\Delta}_{12}*\mathbf{R}_L\right\},\\
v\partial_n\mathbf{T}_L &= -\partial_s\boldsymbol{\Delta}_{11}-v\mathbf{a}^{+}\mathbf{T}_L-\partial_s\left\{(\mathbf{I}+\mathbf{T}_L*)\boldsymbol{\Delta}_{12}*\mathbf{R}_L+\mathbf{T}_L*\boldsymbol{\Delta}_{11}\right\},\\
(v\partial_n+2\partial_s)\mathbf{R}_R &= \partial_s\boldsymbol{\Delta}_{12}+\partial_s\left\{\boldsymbol{\Delta}_{11}*\mathbf{R}_R-\mathbf{R}_R*\boldsymbol{\Delta}_{22}-\mathbf{R}_R*\boldsymbol{\Delta}_{21}*\mathbf{R}_R\right\},\\
v\partial_n\mathbf{T}_R &= -\partial_s\boldsymbol{\Delta}_{22}-v\mathbf{a}^{-}\mathbf{T}_R-\partial_s\left\{(\mathbf{I}+\mathbf{T}_R*)\boldsymbol{\Delta}_{21}*\mathbf{R}_R+\mathbf{T}_R*\boldsymbol{\Delta}_{22}\right\},
\end{aligned}\tag{3.1}$$

and the Green functions equations

$$\begin{aligned}
v\partial_n\mathbf{G}_L^{+} &= \mathbf{G}_L^{+}v\mathbf{a}^{+}+\partial_s\left\{\boldsymbol{\Delta}_{11}+\boldsymbol{\Delta}_{11}*\mathbf{G}_L^{+}+\boldsymbol{\Delta}_{12}*\mathbf{G}_L^{-}\right\},\\
(v\partial_n-2\partial_s)\mathbf{G}_L^{-} &= \mathbf{G}_L^{-}v\mathbf{a}^{+}+\partial_s\left\{\boldsymbol{\Delta}_{21}+\boldsymbol{\Delta}_{21}*\mathbf{G}_L^{+}+\boldsymbol{\Delta}_{22}*\mathbf{G}_L^{-}\right\},\\
(v\partial_n+2\partial_s)\mathbf{G}_R^{+} &= \mathbf{G}_R^{+}v\mathbf{a}^{-}+\partial_s\left\{\boldsymbol{\Delta}_{12}+\boldsymbol{\Delta}_{11}*\mathbf{G}_R^{+}+\boldsymbol{\Delta}_{12}*\mathbf{G}_R^{-}\right\},\\
v\partial_n\mathbf{G}_R^{-} &= \mathbf{G}_R^{-}v\mathbf{a}^{-}+\partial_s\left\{\boldsymbol{\Delta}_{22}+\boldsymbol{\Delta}_{21}*\mathbf{G}_R^{+}+\boldsymbol{\Delta}_{22}*\mathbf{G}_R^{-}\right\}.
\end{aligned}\tag{3.2}$$

These equations also comprise: Initial values on the line $s=0^{+}$, $n\in(0,d)$, see Subsection 4.2.1; Boundary values on the lines $s>0$, $n=0,d$; Finite jump discontinuities propagating from the points $(s,n)=(0^{+},d)$ and $(s,n)=(0^{+},0)$ along the characteristics, see [5]. Physical scattering kernels and the wave front propagators for the entire slab form the complete set of scattering data for a MIP. This set is

$$\begin{aligned}
&\mathbf{R}_L(0,s), \quad \mathbf{T}_L(0,s), \quad \mathbf{Q}^{+}(0,d),\\
&\mathbf{R}_R(d,s), \quad \mathbf{T}_R(d,s), \quad \mathbf{Q}^{-}(d,0).
\end{aligned}\tag{3.3}$$

Alternatively the equivalent set of Green functions can be used, see [5]. In some cases, see appendices B and C, additional data are needed to invert the wave front propagators.

The transformation between the L/R-case equations is found by inspection of the above equations or the dynamics (2.2), cf. [4]. This yields the k_n-transformation[3]

$$\boldsymbol{\Delta}_{kl}(n,s)\to-\boldsymbol{\Delta}_{\overline{k}\,\overline{l}}\,(d-n,s).\tag{3.4}$$

corresponding to $k_n\to-k_n$. Note that ∂ denotes partial derivative, i.e., $\partial_n\to-\partial_n$. The L/R mirror image concept uses only the fact that the $\boldsymbol{\Delta}_{kl}$ dyadics does not depend on the sign of k_n. Due to the explicit forms of Eqs (2.3) and (2.4), there is a similar transformation for $\boldsymbol{k}_{\parallel}\to-\boldsymbol{k}_{\parallel}$. The $\boldsymbol{k}_{\parallel}$-transformation reads

$$\boldsymbol{\Delta}_{kl}(n,s)\to-\boldsymbol{\Delta}_{\overline{k}\,\overline{l}}\,(n,s).$$

Hence, for a homogeneous slab the k_n- and $\boldsymbol{k}_{\parallel}$-transformations are equivalent. It follows that the $\hat{\boldsymbol{k}}$-transformation, corresponding to $\hat{\boldsymbol{k}}\to-\hat{\boldsymbol{k}}$, is an identity. Moreover, an up/down MIP with $\hat{\boldsymbol{k}}^{\pm}=\pm\boldsymbol{k}_{\parallel}+k_n\hat{\boldsymbol{n}}$ can be used alternatively, cf. [4]. In the remaining part of this paper the notation of a left/right MIP is used.

There is also a connection between the imbedding and the Green functions method, see [5], that will be used later.

[3]The bar denotes the dual index defined by $\overline{1}=2$, $\overline{2}=1$, $\overline{m}=e$ and $\overline{e}=m$.

4 The inverse problem

The inverse problem is divided into two parts: the DIP and the RIP. The DIP (Dynamics Inverse Problem) is to reconstruct the $\boldsymbol{\Delta}_{kl}$-dyadics from complete scattering data from a MIP and the RIP (Retrieval of Interior Parameters) is the remaining reconstruction of the susceptibility dyadics $\boldsymbol{\chi}_{e,m}$.

4.1 Retrieval of Interior Parameters: RIP

The input data to the RIP are the $\boldsymbol{\Delta}_{kl}$-dyadics and the output data are the susceptibility dyadics $\boldsymbol{\chi}_{e,m}$. Each set of $\boldsymbol{\Delta}_{kl}$-dyadics corresponds to a given $\boldsymbol{k}_\parallel$, i.e., a MIP.

First, Eq. (2.3) is inverted to get[4] $\mathbf{D}_{\kappa\lambda}$. From the latter set of dyadics the route proceeds in three consecutive steps as depicted in Fig. 3.

In the first step two MIPs (two $\boldsymbol{k}_\parallel$) are used to recover the resolvents L_κ from the $\boldsymbol{k}_\parallel$-dependent parts of $\mathbf{D}_{\kappa\bar{\kappa}}$. This gives the c_κ components via the resolvent equations (2.1).

In the second step a MIP with $\boldsymbol{k}_\parallel \neq \mathbf{0}$ is needed. From the known quantities $\boldsymbol{k}_\parallel$, $\boldsymbol{k}_\parallel \cdot \mathbf{D}_{\kappa\kappa} \cdot \boldsymbol{k}_\parallel$, $(\hat{\boldsymbol{n}} \times \boldsymbol{k}_\parallel) \cdot \mathbf{D}_{\kappa\kappa} \cdot (\hat{\boldsymbol{n}} \times \boldsymbol{k}_\parallel)$ and the resolvents L_κ, obtained in step one, the projections $\boldsymbol{a}_\kappa \cdot \boldsymbol{k}_\parallel$ and $\boldsymbol{b}_\kappa \cdot \boldsymbol{k}_\parallel$ are obtained[5] by using (2.1). Therefore, two MIPs with non-parallel $\boldsymbol{k}_\parallel$ are needed to recover the vectors $\boldsymbol{a}_\kappa$ and $\boldsymbol{b}_\kappa$.

Now, the third step is simply to calculate $\boldsymbol{\chi}_{\parallel,\kappa}$ from $\mathbf{D}_{\bar{\kappa}\kappa}$ using the results from step one and two.

The most narrow passage is step two. Here $\boldsymbol{k}_\parallel^{(1,2)}$ of the two MIPs must satisfy the MIP condition

$$\boldsymbol{k}_\parallel^{(1)} \times \boldsymbol{k}_\parallel^{(2)} \neq \mathbf{0}. \tag{4.1}$$

With this condition on the MIPs the RIP is well posed. This is so since each step in the RIP route is nothing but algebraic manipulations and solution of Volterra equations of the second kind. Note that oblique incidence is crucial to get the resolvents which are the keys to the first and the second step. Normal incidence is useful for mirror image symmetric media and give $\boldsymbol{\chi}_{\parallel,e}$ and $\boldsymbol{\chi}_{\parallel,m}$, see [4]. For media with purely electric or magnetic dispersion ($\boldsymbol{\chi}_m \equiv \mathbf{0}$ or $\boldsymbol{\chi}_e \equiv \mathbf{0}$) one MIP is enough due to simplifications in the second step.

4.2 The Dynamics Inverse Problem: DIP

The remaining problem is to determine the $\boldsymbol{\Delta}_{kl}$ dyadics in (2.2). In this part (DIP) of the inverse problem the specific form of the $\boldsymbol{\Delta}_{kl}$ dyadics can be ignored. Only the magnitude $|\boldsymbol{k}_\parallel|$ enter via the phase velocity v. The input data is the complete

[4] Latin indices are used for 1 and 2 and Greek indices for e and m.

[5] Note that the cross-terms, $(\hat{\boldsymbol{n}} \times \boldsymbol{k}_\parallel) \cdot \mathbf{D}_{\kappa\kappa} \cdot \boldsymbol{k}_\parallel$ and $\boldsymbol{k}_\parallel \cdot \mathbf{D}_{\kappa\kappa} \cdot (\hat{\boldsymbol{n}} \times \boldsymbol{k}_\parallel)$, yield non-invertible quantities.

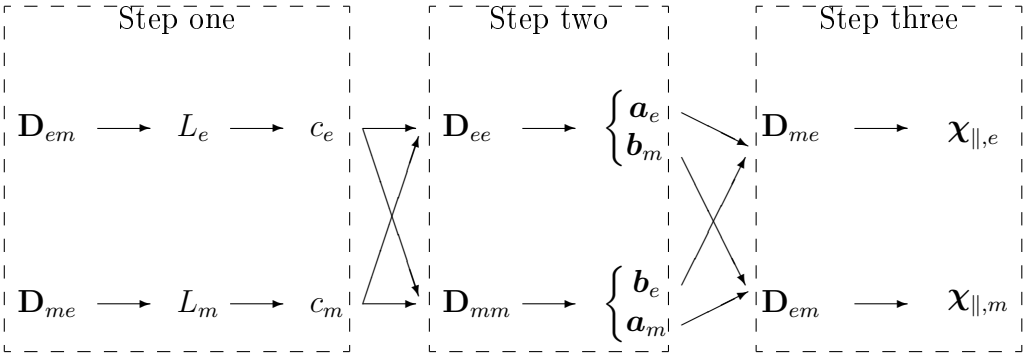

Figure 3: The RIP route.

set of scattering data (3.3) from a MIP. In the DIP for a general anisotropic homogeneous medium complete scattering data from the entire MIP must be used[6]. In the following two subsections the initial values and an iterative algorithm solving the DIP are given.

4.2.1 Initial values for the DIP

The initial values $\mathbf{\Delta}_{kl}(0^+)$ are obtained from the wave front propagators and the initial values of the reflection kernels

$$\begin{aligned}
&\mathbf{\Delta}_{11}(0^+) = \frac{v}{d}\ln\left(\mathbf{Q}^+(0,d)\right), \qquad \mathbf{\Delta}_{22}(0^+) = -\frac{v}{d}\ln\left(\mathbf{Q}^-(d,0)\right),\\
&\mathbf{\Delta}_{21}(0^+) = -2\mathbf{R}_L(0,0^+), \qquad \mathbf{\Delta}_{12}(0^+) = 2\mathbf{R}_R(d,0^+),
\end{aligned}$$

see Appendix B. The initial values for $\partial_s\mathbf{\Delta}_{kk}$ are obtained from the initial values of the transmission kernels

$$\begin{aligned}
\mathbf{T}_L(0,0^+) &= \frac{1}{v}\int_0^d \mathbf{Q}^+(n',0)\left\{\partial_s\mathbf{\Delta}_{11}(0^+) - \frac{1}{2}\mathbf{\Delta}_{12}(0^+)\mathbf{\Delta}_{21}(0^+)\right\}\mathbf{Q}^+(0,n')\,\mathrm{d}n',\\
\mathbf{T}_R(d,0^+) &= \frac{1}{v}\int_0^d \mathbf{Q}^-(n',d)\left\{-\partial_s\mathbf{\Delta}_{22}(0^+) - \frac{1}{2}\mathbf{\Delta}_{21}(0^+)\mathbf{\Delta}_{12}(0^+)\right\}\mathbf{Q}^-(d,n')\,\mathrm{d}n',
\end{aligned}$$

see Appendix C. The remaining values are obtained from the imbedding equations (3.1) for the reflection kernels. The reflection kernel $\mathbf{R}_L$ is n-independent for $s < 2(d-n)/v$ and $\mathbf{R}_R$ is n-independent in the mirror image region. This can be used at the points $(n,s) = (0,0^+)$ and $(d,0^+)$

$$\begin{aligned}
\partial_s\mathbf{\Delta}_{21}(0^+) &= -2\partial_s\mathbf{R}_L(0,0^+) - \mathbf{\Delta}_{22}(0^+)\mathbf{R}_L(0,0^+) + \mathbf{R}_L(0,0^+)\mathbf{\Delta}_{11}(0^+),\\
\partial_s\mathbf{\Delta}_{12}(0^+) &= 2\partial_s\mathbf{R}_R(d,0^+) - \mathbf{\Delta}_{11}(0^+)\mathbf{R}_R(d,0^+) + \mathbf{R}_R(d,0^+)\mathbf{\Delta}_{22}(0^+).
\end{aligned}$$

[6] In the case of mirror image symmetric media see [4] and for reciprocal media see Subsection 5.2.

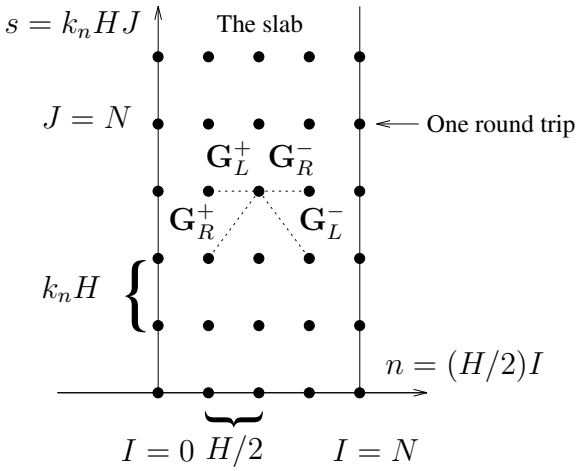

Figure 4: The grid ($N = 5$, length unit d and time unit d/c_0) with N points in the n-direction and per round-trip $s = 2d/v$. Dashed lines indicate the characteristics of the Green functions in the MIPE.

The unique solubility of the equations using transmission data depend on the properties of the eigenvalues of the wave front propagators, see Appendices B and C. If these eigenvalues are real the solution is unique. Otherwise the solution is non-unique or even worse, there may be no solution at all. Note, for reciprocal media the wave front propagators are symmetric, see Subsection 5.2, and hence the eigenvalues are real.

4.2.2 Iterative algorithm for the DIP

In this section an iterative algorithm generating $\mathbf{\Delta}_{kl}(s)$ at arbitrary time is presented. The algorithm is based on the Green functions equations (3.2) and uses data from one MIP.

The Green functions equations are integrated along the characteristics between two consecutive grid points, see Fig. 4, and the time convolutions are approximated using the trapezoidal rule. The discretized equations yield a linear relation between the Green functions and the time derivatives $\mathbf{\Delta}'_{kl}(s)$. It is convenient to use the notation

$$\mathrm{d}\mathbf{\Delta}_{kl}(J) = k_n H \mathbf{\Delta}'_{kl}(k_n HJ).$$

Here, time $s = (k_n H)J$ for time indices $J \leq 0$ and $n = (H/2)I$ for $I = 0, 1, \ldots, N$. With this grid one roundtrip ($s = 2d/v$) is $J = N$.

For the boundary-values of the Green functions, corresponding to physical scattering kernels, the following relation holds

$$
\begin{aligned}
\overrightarrow{\mathbf{G}_L^{+}}(N,J) &= \sum_{k,l=1}^{2} \mathbf{M}_{kl}^{L}(N)\overrightarrow{\mathrm{d}\boldsymbol{\Delta}_{kl}}(J) + \overrightarrow{\mathbf{g}_L^{+}}(N,J),\\
\overrightarrow{\mathbf{G}_L^{-}}(0,J) &= \sum_{k=1}^{2} \mathbf{N}_{2k}^{L}(0)\overrightarrow{\mathrm{d}\boldsymbol{\Delta}_{2k}}(J) + \overrightarrow{\mathbf{g}_L^{-}}(0,J),\\
\overrightarrow{\mathbf{G}_R^{+}}(N,J) &= \sum_{k=1}^{2} \mathbf{N}_{1k}^{R}(N)\overrightarrow{\mathrm{d}\boldsymbol{\Delta}_{1k}}(J) + \overrightarrow{\mathbf{g}_R^{+}}(N,J),\\
\overrightarrow{\mathbf{G}_R^{-}}(0,J) &= \sum_{k,l=1}^{2} \mathbf{M}_{kl}^{R}(0)\overrightarrow{\mathrm{d}\boldsymbol{\Delta}_{kl}}(J) + \overrightarrow{\mathbf{g}_R^{-}}(0,J).
\end{aligned}
\tag{4.2}
$$

Here a 4×4 matrix notation is used, see Appendix A. At any time (index J) $\mathbf{M}$, $\mathbf{N}$ and $\overrightarrow{\mathbf{g}}$ can be calculated if the medium parameters $\mathrm{d}\boldsymbol{\Delta}_{kl}$ are known for all earlier times (time index $< J$). This is done by a formal solution of the direct problem at time index J, see Appendix D. Careful inspection of the results in Appendix D shows that the **M**s and the **N**s depend only on the initial values, as the notation suggests. This is used to optimize the inverse algorithm. A similar algorithm was first used in [3] and it is therefore called the Optimized Karlsson Algorithm (see also [11]).

The Optimized Karlsson Algorithm is:

Time step zero, $J = 0$:
Calculate the initial values $\boldsymbol{\Delta}_{kl}(0^+)$ and $\mathrm{d}\boldsymbol{\Delta}_{kl}(0^+)$, see Section 4.2.1. Convert the scattering data to Green functions, see [5], and calculate the initial values of the Green functions inside the slab $0 < I < N$. Furthermore, the jump discontinuities in $\mathbf{G}_L^-$ and $\mathbf{G}_R^+$ can be calculated [5].

Time step one, $J = 1$:
Truncate the medium at $J = 1$, i.e., let $\mathrm{d}\boldsymbol{\Delta}_{kl}(1) = \mathbf{0}$, and calculate the truncated Green functions $\mathbf{g}$ for $J = 1$ by running the forward program twice (L and R case). Calculate the matrices $\mathbf{M}$ and $\mathbf{N}$ by a 16-fold variation of $\mathrm{d}\boldsymbol{\Delta}_{kl}(1)$ and running the forward program 2×16 times. Solve for $\mathrm{d}\boldsymbol{\Delta}_{kl}(1)$ using Eq. (4.2). Finally, calculate the Green functions inside the slab $0 < I < N$ at $J = 1$ by running the forward program twice (L and R case).

General time step, $J \geq 1$:
Truncate the medium, i.e., let $\mathrm{d}\boldsymbol{\Delta}_{kl}(J) = \mathbf{0}$, and calculate the truncated Green functions $\mathbf{g}$ at time index J by running the forward program twice (L and R case). Use (4.2), the true and the truncated Green functions to calculate $\mathrm{d}\boldsymbol{\Delta}_{kl}(J)$. Calculate the Green functions inside the slab $0 < I < N$ at J by running the forward program twice (L and R case). Repeat the general time step at the next time index. The algorithm is closed.

Note that the forward program is executed 34 times in time step one. By using the domain of dependence results in Appendix D only 2 times are needed in the

following time steps. As the total number of time steps increases this trick speeds up the code roughly by a factor $34/2 = 17$.

5 Constraints and simplifications

The total DIP-RIP algorithm is a map from 32 to 18 scalar functions (from two MIPs to two susceptibility dyadics) and 14 zeros due to the specific form of the anisotropic constitutive relations (it is not an arbitrarily complex medium). These zeros enter as implicit constraints in the scattering data via the imbedding or the Green functions equations and they are therefore very hard to translate to explicit constraints in the scattering data. For some subclasses of anisotropic media there are explicit constraints in the scattering data and simplifications in the inversion algorithm.

5.1 Purely electric or magnetic dispersion

For a medium with purely electric or magnetic dispersion ($\boldsymbol{\chi}_m \equiv \mathbf{0}$ or $\boldsymbol{\chi}_e \equiv \mathbf{0}$) only one MIP is needed due to simplifications in the second step in the RIP route, see Section 4.1.

5.2 Reciprocal media

For reciprocal media[7], Eqs (2.4) and (2.3) yield

$$\boldsymbol{\Delta}_{kk} = \boldsymbol{\Delta}_{kk}^T, \qquad \boldsymbol{\Delta}_{k\overline{k}} = -\boldsymbol{\Delta}_{\overline{k}k}^T. \tag{5.1}$$

Here T denotes transponation and $\overline{k}$ and k are dual indices. The coupling between the $\boldsymbol{\Delta}_{k\overline{k}}$-dyadics yields the reciprocity relation for homogeneous media

$$\mathbf{R}_L(n,s) = \{\mathbf{R}_R(d-n,s)\}^T,$$

which follows from the assumed unique solubility of Eq. (3.1). If furthermore $\boldsymbol{a}_e(s)\times \boldsymbol{k}_\parallel \equiv \boldsymbol{a}_m(s)\times\boldsymbol{k}_\parallel \equiv \mathbf{0}$ then the reflection kernels are symmetric. There is also a similar relation for the wave front propagators

$$\mathbf{Q}^\pm(n_1,n_2) = \{\mathbf{Q}^\pm(n_1,n_2)\}^T.$$

The transmission kernels are in general not symmetric. To see this calculate the derivatives $\partial_s^n \mathbf{T}_{R,L}(n,0^+) \quad n = 0,1,\ldots$ iteratively using the imbedding equations. For $n = 0$ symmetry follows from (5.1) and for $n = 1$ $\boldsymbol{\Delta}_{kl}(0^+) = \mathbf{0}$ is needed. In that case $\partial_s \boldsymbol{\Delta}_{kl}(0^+) \neq \mathbf{0}$. This is needed to have a passive medium, i.e., no electromagnetic energy is created by the medium itself, see [8]. Lengthy but straightforward calculations show that the cases $n = 2,3$ are symmetric and $n = 4$ contains

[7] A reciprocal medium is defined as a medium having symmetric susceptibility dyadics, see [8].

28 symmetric components and one antisymmetric component. The antisymmetric component (L case) is[8]

$$\left\{\partial_s^4 \mathbf{T}_L(n,0^+)\right\}^a = \frac{d-n}{4v}\left[\boldsymbol{\Delta}'_{11}(0^+)\boldsymbol{\Delta}'_{12}(0^+)\boldsymbol{\Delta}'_{21}(0^+) - \boldsymbol{\Delta}'_{12}(0^+)\boldsymbol{\Delta}'_{21}(0^+)\boldsymbol{\Delta}'_{11}(0^+)\right],$$

which is not zero in general.

5.3 Mirror image symmetric media

A medium is mirror image symmetric if $\mathbf{D}_{ee} \equiv \mathbf{D}_{mm} \equiv \mathbf{0}$, see Eq. (3.4) and [4]. For a medium with purely electric or magnetic dispersion this is equivalent to $\boldsymbol{a}_\kappa \equiv \boldsymbol{b}_\kappa \equiv \mathbf{0}$. For general media the same holds if mirror image symmetry is considered for two MIPs with the MIP condition (4.1). This is so since each MIP require $\boldsymbol{a}_\kappa \cdot \boldsymbol{k}_\parallel \equiv \boldsymbol{b}_\kappa \cdot \boldsymbol{k}_\parallel \equiv 0$. For mirror image symmetric media the L and R case equations are identical and one of them can be dropped.

6 Numerical experiments

To illustrate the analysis, two numerical examples are presented. In both examples, the medium is reciprocal ($\boldsymbol{\chi}^T_{\parallel,e} = \boldsymbol{\chi}_{\parallel,e}$ and $\boldsymbol{a}_e = \boldsymbol{b}_e$), mirror-image-asymmetrical ($\boldsymbol{a}_e \neq \mathbf{0}$) and without magnetic dispersion ($\boldsymbol{\chi}_m \equiv \mathbf{0}$). Hence, the same simplified RIP route is used. The reciprocity relations in Subsection 5.2 have not been used to simplify the inversion algorithm, they have merely been used to check the output. To avoid inversion bias the imbedding method, cf. Ref. [5], is used to generate the direct scattering data and the inverse problem uses the Green functions method and the optimized Karlsson algorithm, see Sections 4.2.1 and 4.2.2. In the imbedding approach the scattering kernels are defined for a sub-slab imbedded in vacuum whereas in the Green functions method the physical slab is used. Using the imbedding method the scattering kernels for the sub-slab do not generate the internal fields which is the case in the Green functions method [5]. Therefore, in a comparison between the methods, the scattering kernels inside the slab are different. These internal values are used in the Karlsson method.

In order to present the numerical results, coordinate systems are introduced. The slab system is a fixed right-handed Cartesian coordinate system with basis vectors $\hat{\boldsymbol{e}}_1$, $\hat{\boldsymbol{e}}_2$ in the planes of stratification and $\hat{\boldsymbol{e}}_1 \times \hat{\boldsymbol{e}}_2 = \hat{\boldsymbol{e}}_3 = \hat{\boldsymbol{n}}$. In this system the susceptibility kernel $\boldsymbol{\chi}_e$ is represented by the 3×3 matrix $[\boldsymbol{\chi}_e]$. Explicitly

$$[\boldsymbol{\chi}_e] = \begin{bmatrix} \chi^e_{11} & \chi^e_{12} & \chi^e_{13} \\ \chi^e_{21} & \chi^e_{22} & \chi^e_{23} \\ \chi^e_{31} & \chi^e_{32} & \chi^e_{33} \end{bmatrix} = \begin{bmatrix} \hat{\boldsymbol{e}}_1 \cdot \boldsymbol{\chi}_e \cdot \hat{\boldsymbol{e}}_1 & \hat{\boldsymbol{e}}_1 \cdot \boldsymbol{\chi}_e \cdot \hat{\boldsymbol{e}}_2 & \hat{\boldsymbol{e}}_1 \cdot \boldsymbol{\chi}_e \cdot \hat{\boldsymbol{e}}_3 \\ \hat{\boldsymbol{e}}_2 \cdot \boldsymbol{\chi}_e \cdot \hat{\boldsymbol{e}}_1 & \hat{\boldsymbol{e}}_2 \cdot \boldsymbol{\chi}_e \cdot \hat{\boldsymbol{e}}_2 & \hat{\boldsymbol{e}}_2 \cdot \boldsymbol{\chi}_e \cdot \hat{\boldsymbol{e}}_3 \\ \hat{\boldsymbol{e}}_3 \cdot \boldsymbol{\chi}_e \cdot \hat{\boldsymbol{e}}_1 & \hat{\boldsymbol{e}}_3 \cdot \boldsymbol{\chi}_e \cdot \hat{\boldsymbol{e}}_2 & \hat{\boldsymbol{e}}_3 \cdot \boldsymbol{\chi}_e \cdot \hat{\boldsymbol{e}}_3 \end{bmatrix}$$

An angle of incidence θ is defined such that $\hat{\boldsymbol{k}} = \sin\theta\hat{\boldsymbol{e}}_2 + \cos\theta\hat{\boldsymbol{e}}_3$. The principal system is another Cartesian coordinate system rotated with respect to the slab

[8] Here $\boldsymbol{\Delta}'_{kl}(0^+) = \partial_s \boldsymbol{\Delta}_{kl}(0^+)$ and the superscript a denotes antisymmetric part.

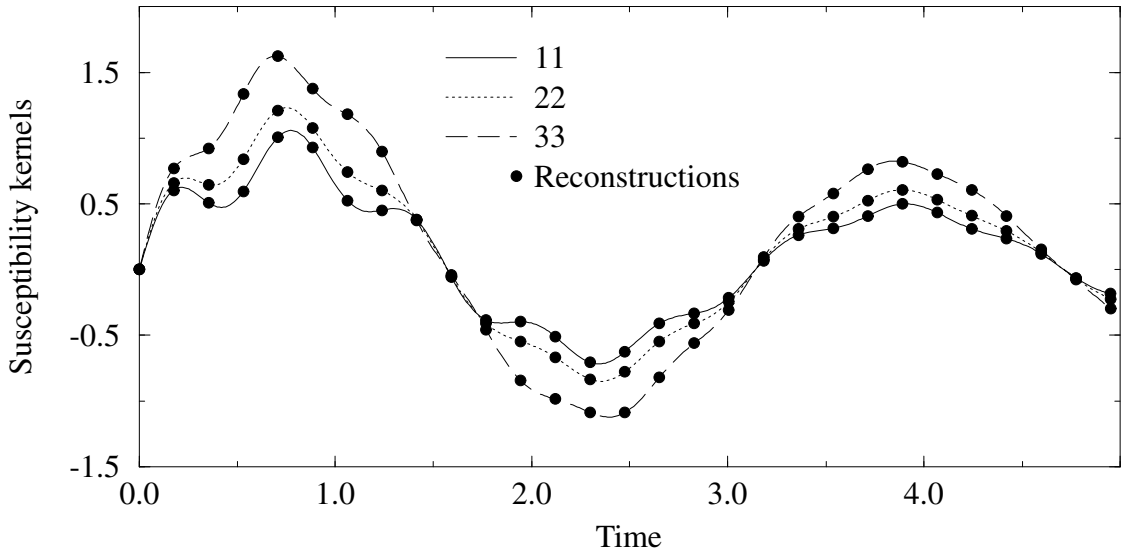

Figure 5: Reconstruction of the diagonal susceptibility kernels χ^e_{11}, χ^e_{22} and χ^e_{33} in Example 1.

system in such a way that the dyadic $\boldsymbol{\chi}_e$ in this coordinate system has a diagonal matrix representation. The transformation between these systems is given by three Euler angles. In the examples below these Euler angles are constant in time. Note that one round trip is $s = 2|\cos\theta|d/c_0$ and in all graphs the horizontal axis is in units of d/c_0 and the vertical axis is in units of c_0/d.

Example 1

The first example is a uniaxial medium. In the principal system $[\boldsymbol{\chi}_e] = \mathrm{diag}(g, g, g_3)$, where

$$g(t) = e^{-0.2t}\sin 2t + 0.3\mathrm{e}^{-0.5t}\sin 10t,$$
$$g_3(t) = 2e^{-0.2t}\sin 2t + 0.2\mathrm{e}^{-0.5t}\sin 12t.$$

The principal system is rotated over an angle $\pi/6$ around the x-axis in the slab system. Reconstructions are made for 3.5 roundtrips using a MIP at oblique incidence and angle of incidence $\pi/4$. Results are depicted in Figs 5 and 6.

Example 2

The second example is a biaxial medium with $[\boldsymbol{\chi}_e] = \mathrm{diag}(g_1, g_2, g_3)$ in the principal system. The explicit forms of the g_i-functions are

$$g_1(t) = 2e^{-0.3t}\sin 4t,$$
$$g_2(t) = e^{-0.3t}\sin 8t,$$
$$g_3(t) = 3e^{-0.3t}\sin 6t.$$

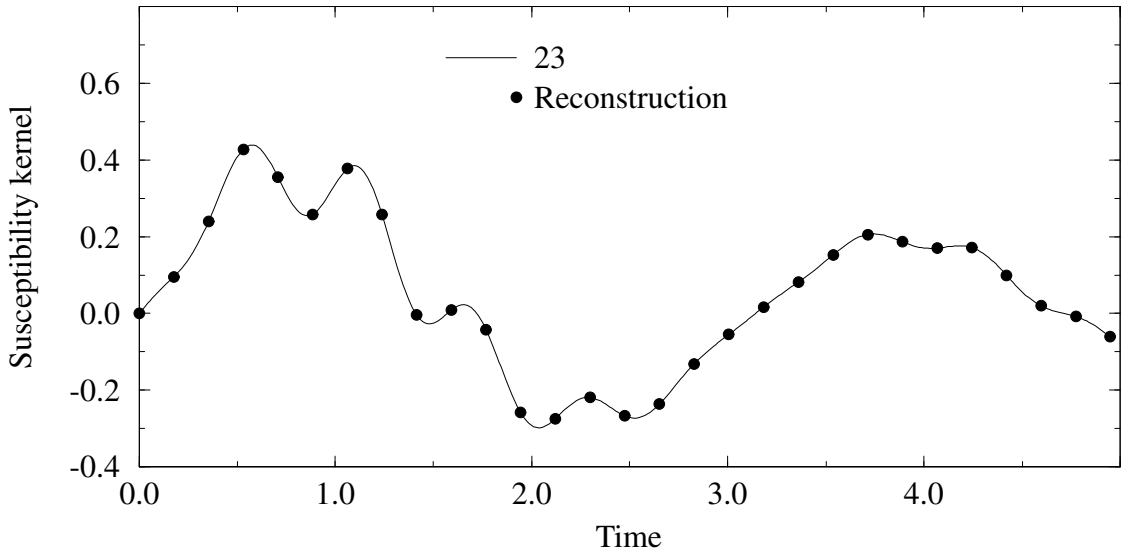

Figure 6: Reconstruction of χ^e_{23} in Example 1.

The Euler angles ϕ, θ and ψ, corresponding to successive rotations around the $\hat{\boldsymbol{e}}_3$-, $\hat{\boldsymbol{e}}_1$-, and $\hat{\boldsymbol{e}}_3$-axes, respectively, are

$$\phi = \pi/6, \qquad \theta = 5\pi/12, \qquad \psi = \pi/4.$$

see [6].

Reconstructions for three roundtrips using a MIP at oblique incidence and angle of incidence $\pi/4$ are depicted in Figs 7 and 8.

To further test the optimized Karlsson algorithm uniform noise has been added to the scattering kernels. Each of the kernels $\mathbf{G}^-_L$, $\mathbf{G}^+_L$, $\mathbf{G}^+_R$ and $\mathbf{G}^-_R$ have been corrupted with uniform noise of the same relative amplitude using the norm

$$\|\mathbf{K}\| = \max_{i,j=1,2,s\geq 0} |\hat{\boldsymbol{e}}_i \cdot \mathbf{K}(s) \cdot \hat{\boldsymbol{e}}_j|,$$

where $\mathbf{K}(s)$ is any of the above kernels. The root mean square signal to noise ratio (SNR) is used to measure the noise in the scattering data. The minimum value (worst case) of the SNRs for all components of the complete set of scattering data is used. The SNR ratio is defined as SNR$= \sigma_D/\sigma_N$ where $\sigma_{D,N}$ are the standard deviations of the data and the noise, respectively. Results are depicted in Figs 9 and 10.

Appendix A 4×4 matrix notation.

All dyadics in this paper, except for $\boldsymbol{\chi}_\kappa$, are two-dimensional. Here, two-dimensional means that $\hat{\boldsymbol{n}} \cdot \mathbf{D} = \mathbf{D} \cdot \hat{\boldsymbol{n}} = \mathbf{0}$ for any dyadic $\mathbf{D}$. To solve the equations it is useful to introduce a 4×4 matrix notation. First introduce orthonormal basis vectors $\hat{\boldsymbol{e}}_1$

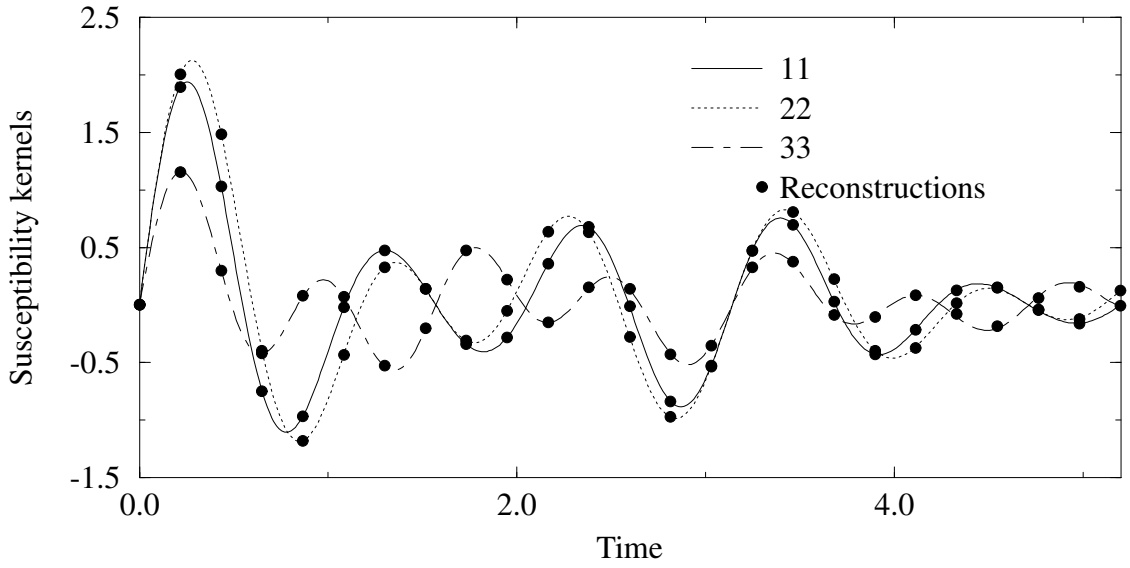

Figure 7: Reconstruction of the diagonal susceptibility kernels χ^e_{11}, χ^e_{22} and χ^e_{33} in Example 2.

and $\hat{\boldsymbol{e}}_2 = \hat{\boldsymbol{n}} \times \hat{\boldsymbol{e}}_1$ in the planes of stratification, i.e., $\hat{\boldsymbol{e}}_1 \cdot \hat{\boldsymbol{n}} = \hat{\boldsymbol{e}}_2 \cdot \hat{\boldsymbol{n}} = 0$. Furthermore, let any two-dimensional dyadic $\mathbf{D}$ be represented by the 2×2 matrix

$$[\mathbf{D}] = \begin{bmatrix} \hat{\boldsymbol{e}}_1 \cdot \mathbf{D} \cdot \hat{\boldsymbol{e}}_1 & \hat{\boldsymbol{e}}_1 \cdot \mathbf{D} \cdot \hat{\boldsymbol{e}}_2 \\ \hat{\boldsymbol{e}}_2 \cdot \mathbf{D} \cdot \hat{\boldsymbol{e}}_1 & \hat{\boldsymbol{e}}_2 \cdot \mathbf{D} \cdot \hat{\boldsymbol{e}}_2 \end{bmatrix} \tag{A.1}$$

or the column-vector

$$\overrightarrow{\mathbf{D}} = \begin{bmatrix} \hat{\boldsymbol{e}}_1 \cdot \mathbf{D} \cdot \hat{\boldsymbol{e}}_1 \\ \hat{\boldsymbol{e}}_2 \cdot \mathbf{D} \cdot \hat{\boldsymbol{e}}_1 \\ \hat{\boldsymbol{e}}_1 \cdot \mathbf{D} \cdot \hat{\boldsymbol{e}}_2 \\ \hat{\boldsymbol{e}}_2 \cdot \mathbf{D} \cdot \hat{\boldsymbol{e}}_2 \end{bmatrix}. \tag{A.2}$$

The direct product "$\otimes$"of 2×2 matrices, see [13], is defined by

$$[\mathbf{A}] \otimes [\mathbf{B}] = \begin{bmatrix} A_{11}\,[\mathbf{B}] & A_{12}\,[\mathbf{B}] \\ A_{21}\,[\mathbf{B}] & A_{22}\,[\mathbf{B}] \end{bmatrix},$$

where $A_{kl} = \hat{\boldsymbol{e}}_k \cdot \mathbf{A} \cdot \hat{\boldsymbol{e}}_l$. This is used to obtain the 4-vector representations for dyadic products

$$\begin{aligned} \overrightarrow{\mathbf{A} \cdot \mathbf{B}} &= ([\mathbf{I}_\parallel] \otimes [\mathbf{A}])\overrightarrow{\mathbf{B}} = ([\mathbf{B}]^T \otimes [\mathbf{I}_\parallel])\overrightarrow{\mathbf{A}}, \\ \overrightarrow{\mathbf{A} \cdot \mathbf{B} \cdot \mathbf{C}} &= ([\mathbf{C}]^T \otimes [\mathbf{A}])\overrightarrow{\mathbf{B}}. \end{aligned}$$

Here $[\mathbf{I}_\parallel]$ is the 2×2 identity matrix and T denotes the transposed matrix.

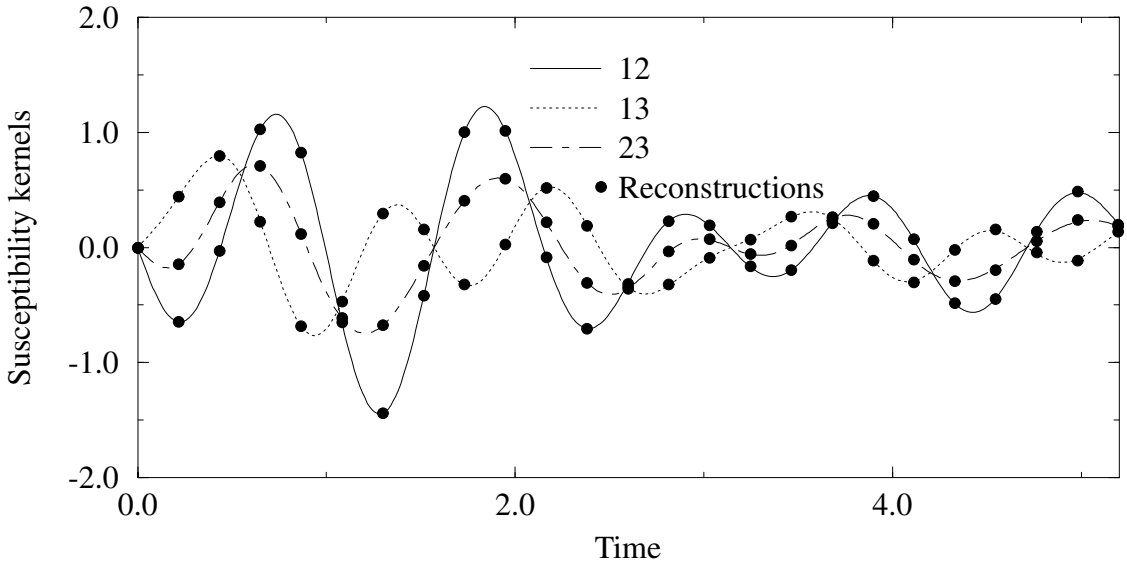

Figure 8: Reconstruction of the off diagonal susceptibility kernels χ^e_{12}, χ^e_{13} and χ^e_{23} in Example 2.

Appendix B Logarithm of the Wave Front Propagator

The wave front propagators have the form $\mathbf{a} = \exp \mathbf{b}$ where $\mathbf{a}$ and $\mathbf{b}$ are real two-dimensional dyadics, see Appendix A. In the inverse problem $\mathbf{a}$ is known and $\mathbf{b}$ is the unknown. The formal solution to this problem is $\mathbf{b} = \ln \mathbf{a}$. This is the solution if $z = \ln \exp z$ for any z in[9] $\mathrm{sp}(\mathbf{b})$, see, e.g. [7, p. 11]. Note, the eigenvalues of $\mathbf{b}$ and $\mathbf{a}$ are either real or complex-conjugated and $\mathrm{sp}(\mathbf{a}) = (\exp z_1, \exp z_2)$ where $\mathrm{sp}(\mathbf{b}) = (z_1, z_2)$.

By inspection of the different possibilities for $\mathrm{sp}(\mathbf{a})$ the solubility of the equation separates into three cases.

Real non-degenerate $\mathrm{sp}(\mathbf{a})$: Unique solution with real non-degenerate spectrum.

Complex $\mathrm{sp}(\mathbf{a})$: Non-unique solution with complex spectrum. One of the solutions is the correct one.

Degenerate (real) $\mathrm{sp}(\mathbf{a})$: Unique solution with degenerate spectrum. This is the correct solution only if $\mathrm{sp}(\mathbf{b})$ is degenerate. Note, $\mathrm{sp}(\mathbf{b})$ is mapped into the real axis.

To see the underlying physics the explicit forms are presented. The Cayley-Hamilton theorem [12, 13] is used to reduce the power series of the exponential and the logarithm

[9] Here $\mathrm{sp}(\mathbf{b})$ denotes the spectrum of $\mathbf{b}$.

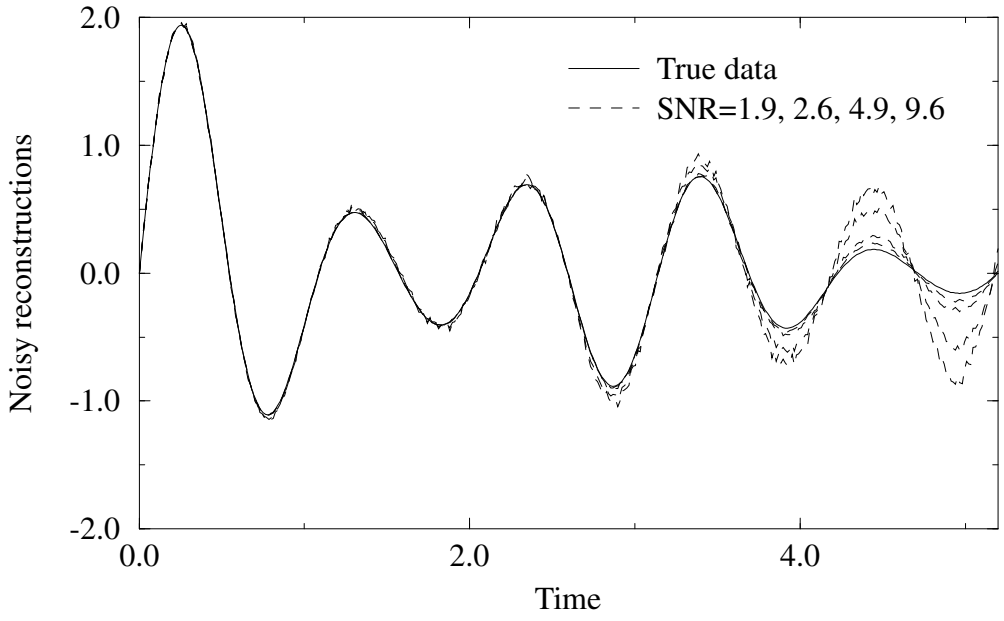

Figure 9: Convergence as SNR increases for the reconstruction of χ^e_{11} in Example 2.

$$\begin{aligned} \exp \mathbf{b} &= \exp(b_0)[\cosh(\widetilde{b})\mathbf{I}_\parallel + \sinh(\widetilde{b})\widetilde{\mathbf{b}}/\widetilde{b}], \\ \ln \mathbf{a} &= \frac{1}{2}\ln(a_0^2 - \widetilde{a}^2)\mathbf{I}_\parallel + \frac{1}{2}\ln\left(\frac{a_0+\widetilde{a}}{a_0-\widetilde{a}}\right)\frac{\widetilde{\mathbf{a}}}{\widetilde{a}}. \end{aligned} \tag{B.1}$$

Here the dyadics are decomposed into a trace-part and a trace-less part using the notation $\mathbf{a} = a_0\mathbf{I}_\parallel + \widetilde{\mathbf{a}}$, $\mathrm{sp}(\mathbf{a}) = (a_0 + \widetilde{a}, a_0 - \widetilde{a})$ where $\det\widetilde{\mathbf{a}} = -\widetilde{a}^2$.

The above three cases correspond to: $\mathrm{Re}\,\widetilde{a} \neq 0$, $\mathrm{Im}\,\widetilde{a} \neq 0$ and $\widetilde{a} = 0$. In the first case the wave front is rotated less than π and it is always possible to solve $\mathbf{a} = \exp\mathbf{b}$ without ambiguity. In the second case, the wave front propagator comprises an oscillating part and the number of oscillations is in principle unknown. Therefore, there are infinitely many solutions, each corresponding to a given number of oscillations or, equivalently, a particular choice of branch for the scalar logarithm function. In the last case the wave front is rotated an integer multiple of π. Therefore, the wave front propagator resembles that of an isotropic medium experiment at normal incidence. This implies that if $\widetilde{\mathbf{b}} \neq \mathbf{0}$ then important data is hidden and cannot be recovered.

Note, the trace $2b_0$ can always be recovered via the formula $a_0^2 - \widetilde{a}^2 = \det\exp\mathbf{b} = \exp 2b_0$. The possible non-solubility of the equation is due to the trace-less parts of Eq. (B.1). For reciprocal media, see Sec. 5, the relevant $\mathbf{b}$:s are symmetric. Hence, $\mathrm{sp}(\mathbf{b})$ is real and the degenerate case corresponds to $\widetilde{\mathbf{a}} = \widetilde{\mathbf{b}} = \mathbf{0}$. Therefore, for reciprocal media the solution is unique.

For homogeneous dispersive media the dyadic $\mathbf{b}$ has the form $\mathbf{b} = \mathbf{c}d$ where d is the thickness of the slab and $\mathbf{c}$ depends on $\boldsymbol{k}_\parallel$, $\boldsymbol{\chi}_e(0^+)$ and $\boldsymbol{\chi}_m(0^+)$. For fixed medium parameters and thickness of the slab, the non-soluble cases are given by

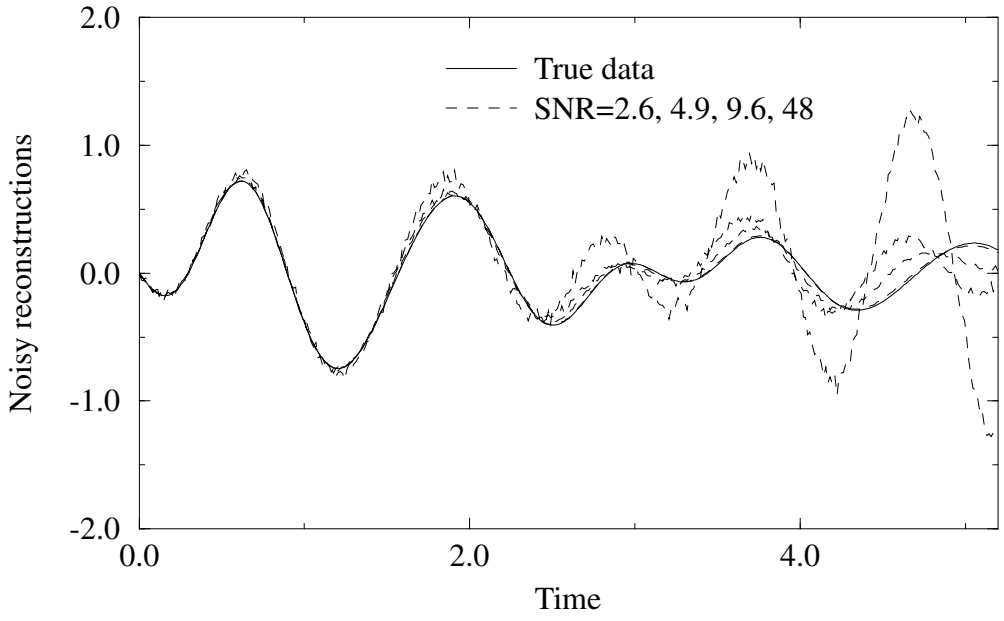

Figure 10: Convergence as SNR increases for the reconstruction of χ^e_{23} in Example 2.

$$\operatorname{Im}\widetilde{c}(\boldsymbol{k}_\parallel;\boldsymbol{\chi}_e(0^+),\boldsymbol{\chi}_m(0^+)) = m\pi/d \qquad m = 1,2,\dots\,, \tag{B.2}$$

This equation yields a collection of $\boldsymbol{k}_\parallel$ on the disc $|\boldsymbol{k}_\parallel| < 1$. Each m corresponds to a curve of solutions $\boldsymbol{k}_\parallel = \sin\theta(\cos\phi\hat{\boldsymbol{e}}_1 + \sin\phi\hat{\boldsymbol{e}}_2)$. Here, $\hat{\boldsymbol{e}}_1$ and $\hat{\boldsymbol{e}}_2$ are orthonormal basis vectors in the planes of stratification, see Appendix A. As d goes to infinity (thick slab) these curves come close to each other and fill up whole sectors or possibly the whole unit-disc. On the other hand as d becomes small (thin slab) the solution curves separate. At the edge ($|\boldsymbol{k}_\parallel| = 1$) $\operatorname{Im}\widetilde{c}$ may diverge and in that case $d = 0^+$ is needed near the edge ($|\boldsymbol{k}_\parallel| = 1^-$).

Below, the numerical solution of (B.2) is depicted in a number of cases. To the left $\operatorname{Im}\widetilde{c}(\boldsymbol{k}_\parallel)$ is depicted and in the middle the solution curves are indicated. In the white regions $\operatorname{Im}\widetilde{c}(\boldsymbol{k}_\parallel) < \pi/d$ and in the neighboring regions (first gray-level) $\pi/d < \operatorname{Im}\widetilde{c}(\boldsymbol{k}_\parallel) < 2\pi/d$ etc. Hence, in the white region the wave front is rotated less than π and the solution is unique. Numerical values uses the length unit d_0 and the frequency unit c_0/d_0. The boundary $|\boldsymbol{k}_\parallel| = 1$ is indicated by a dashed line and the orientation of the basis vector $\hat{\boldsymbol{e}}_1$ is depicted in Fig. 11. For the matrix representation of the susceptibility dyadics see Section 6.

Appendix C Solution of a dyadic equation

The objective here is to solve for **b** in the equation

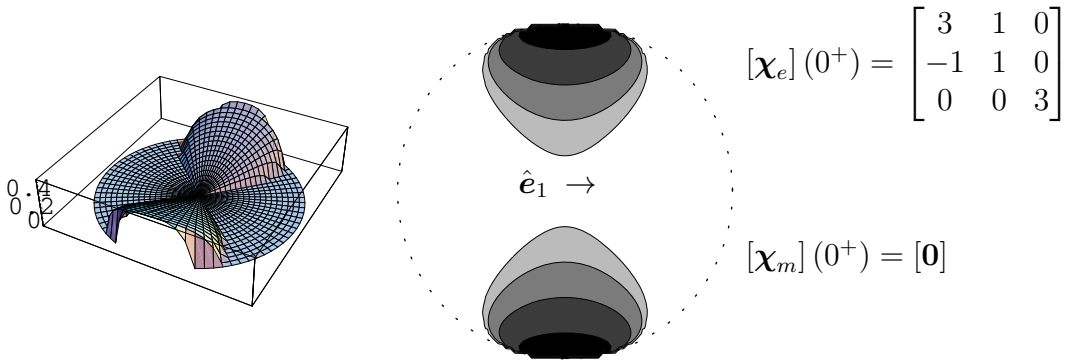

Figure 11: In the first example $d = 30d_0$ and the initial data is mirror image symmetrical. The solution is non-unique in two sectors.

$$\mathbf{a} = \int_0^z \exp(-\mathbf{c}z')\mathbf{b}\exp(\mathbf{c}z')\mathrm{d}z', \tag{C.1}$$

where $\mathbf{a}$, $\mathbf{b}$ and $\mathbf{c}$ are two-dimensional dyadics. This equation is solved by using Equation (B.1) and the 4×4 matrix notation introduced in Appendix A. The formal solution to Eq. (C.1) is $\overrightarrow{\mathbf{b}} = \mathcal{W}^{-1}\overrightarrow{\mathbf{a}}$ where

$$\mathcal{W} = \frac{\mathrm{f}^+(\widetilde{c}z)}{\widetilde{c}}([\mathbf{I}_\parallel] \otimes [\mathbf{I}_\parallel]) + \frac{\mathrm{g}(\widetilde{c}z)}{\widetilde{c}^2}\left\{([\widetilde{\mathbf{c}}]^T \otimes [\mathbf{I}_\parallel]) - ([\mathbf{I}_\parallel] \otimes [\widetilde{\mathbf{c}}])\right\} + \frac{\mathrm{f}^-(\widetilde{c}z)}{\widetilde{c}^3}([\widetilde{\mathbf{c}}]^T \otimes [\widetilde{\mathbf{c}}]),$$
$$\mathrm{f}^\pm(x) = \frac{1}{2}(x \pm \cosh x \sinh x), \qquad \mathrm{g}(x) = \frac{1}{2}\sinh^2 x.$$

The eigenvalues γ_i of $\mathcal{W}$ are related to the eigenvalues $\pm\widetilde{c}$ of $\widetilde{\mathbf{c}}$, see Ref. [13]. Explicitly

$$\gamma_{1,2}(z) = z, \qquad \gamma_{3,4} = \mathrm{h}^\pm(z),$$
$$\mathrm{h}^\pm(z) = \frac{\sinh(\widetilde{c}z)}{\widetilde{c}}(\cosh(\widetilde{c}z) \pm \frac{1}{2}\sinh(\widetilde{c}z)).$$

If $\mathrm{Im}\,\widetilde{c} = 0$ both functions $\mathrm{h}^\pm(n)$ have positive definite z-derivative and therefore $\gamma_i = 0$ if and only if $z = 0$. If $\mathrm{Im}\,\widetilde{c} \neq 0$ then $\mathrm{h}^\pm(n)$ are periodic functions and $\gamma_{3,4}$ are complex values on ellipses, see Fig. 14.

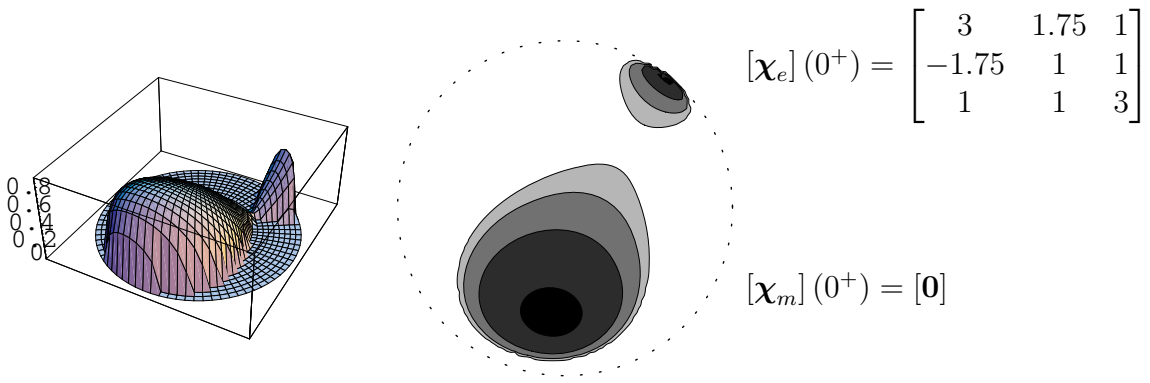

Figure 12: In the second example $d = 15d_0$ and the initial data is not mirror image symmetrical. The solution is non-unique in two sectors.

In this case zero eigenvalues are obtained for $\mathrm{Im}\,\widetilde{c} = m\pi/z \quad m = 1, 2, \ldots$ or $z = 0$. Note, this result is identical to Eq. (B.2). Therefore, this is no further restriction on the solubility of the inverse problem.

Appendix D Domain of dependence results

This appendix comprises the solution for $\mathbf{M}^L_{kl}$, $\mathbf{N}^L_{kl}$ and $\mathbf{g}^{\pm}_L$ in Eq. (4.2) (for the R case use (3.4)). At a general point (I, J) inside the slab the discretized equations have the form

$$\begin{aligned} \overrightarrow{\mathbf{G}^+_L}(I,J) &= \sum_{k,l=1}^{2} \mathbf{M}^L_{kl}(I)\overrightarrow{\mathrm{d}\boldsymbol{\Delta}_{kl}}(J) + \overrightarrow{\mathbf{g}^+_L}(I,J), \\ \overrightarrow{\mathbf{G}^-_L}(I,J) &= \sum_{k,l=1}^{2} \mathbf{N}^L_{kl}(I)\overrightarrow{\mathrm{d}\boldsymbol{\Delta}_{kl}}(J) + \overrightarrow{\mathbf{g}^-_L}(I,J), \end{aligned} \tag{D.1}$$

see (A.2) for the notation $\overrightarrow{\mathbf{G}^+_L}$ etc. The linear relationship is a consequence of the form of the general step, from $(I-1, J)$ to (I, J),

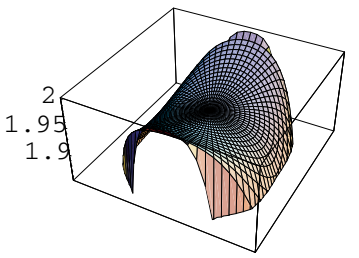

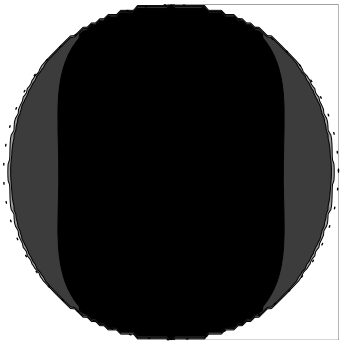

$$[\boldsymbol{\chi}_e]\,(0^+) = \begin{bmatrix} 3 & 2 & 0 \\ -2 & 1 & 0 \\ 0 & 0 & 3 \end{bmatrix}$$

$$[\boldsymbol{\chi}_m]\,(0^+) = \begin{bmatrix} 1 & 2 & 0 \\ -2 & 1 & 0 \\ 0 & 0 & 1 \end{bmatrix}$$

Figure 13: In the last example $d = 5d_0$ and the initial data is mirror image symmetrical. The solution is non-unique for nearly all incident directions.

$$\begin{aligned} \begin{pmatrix} \overrightarrow{\mathbf{G}_L^+}(I,J) \\ \overrightarrow{\mathbf{G}_L^-}(I,J) \end{pmatrix} = \begin{pmatrix} \mathbf{a} & \mathbf{b} \\ \mathbf{c} & \mathbf{d} \end{pmatrix} \Bigg[& \begin{pmatrix} \mathbf{P}_\alpha^\tau(I)\overrightarrow{\mathrm{d}\boldsymbol{\Delta}_{11}}(J) + \mathbf{P}_\alpha^\rho\overrightarrow{\mathrm{d}\boldsymbol{\Delta}_{12}}(J) \\ \mathbf{P}_\beta^\tau(I)\overrightarrow{\mathrm{d}\boldsymbol{\Delta}_{21}}(J) + \mathbf{P}_\beta^\rho\overrightarrow{\mathrm{d}\boldsymbol{\Delta}_{22}}(J) \end{pmatrix} \\ & + \begin{pmatrix} \mathbf{A}^\tau\overrightarrow{\mathbf{G}_L^+}(I-1,J) + \mathbf{A}^\rho\overrightarrow{\mathbf{G}_L^-}(I-1,J) + \overrightarrow{\Sigma}_L^+(I,J) \\ \overrightarrow{\Sigma}_L^-(I,J) \end{pmatrix} \Bigg]. \end{aligned} \tag{D.2}$$

At the boundaries one of the Green functions vanishes. The form of (D.2) is slightly modified

$$\begin{aligned} \mathbf{G}_L^+(0,J) = \mathbf{0} \qquad \text{and} \qquad \begin{pmatrix} \mathbf{a} & \mathbf{b} \\ \mathbf{c} & \mathbf{d} \end{pmatrix} \to \begin{pmatrix} \mathbf{0} & \mathbf{0} \\ \mathbf{0} & \boldsymbol{\delta} \end{pmatrix} \qquad \text{at } I = 0, \\ \mathbf{G}_L^-(N,J) = \mathbf{0} \qquad \text{and} \qquad \begin{pmatrix} \mathbf{a} & \mathbf{b} \\ \mathbf{c} & \mathbf{d} \end{pmatrix} \to \begin{pmatrix} \boldsymbol{\alpha} & \mathbf{0} \\ \mathbf{0} & \mathbf{0} \end{pmatrix} \qquad \text{at } I = N. \end{aligned} \tag{D.3}$$

The explicit forms of $\mathbf{P}_\alpha^\tau(I)$, $\mathbf{P}_\alpha^\rho$, $\mathbf{P}_\beta^\tau(I)$, $\mathbf{P}_\beta^\rho$, $\mathbf{a}$, $\mathbf{b}$, $\mathbf{c}$, $\mathbf{d}$, $\mathbf{A}^\tau$ and $\mathbf{A}^\rho$ are not important for the result in this appendix. Note, however, that these matrices depend only on the initial values $J = 0$, as the J-independent notation suggests. The vectors $\overrightarrow{\Sigma}_L^\pm$ represent the memory of the medium, i.e., they depend only on earlier times (time index $< J$).

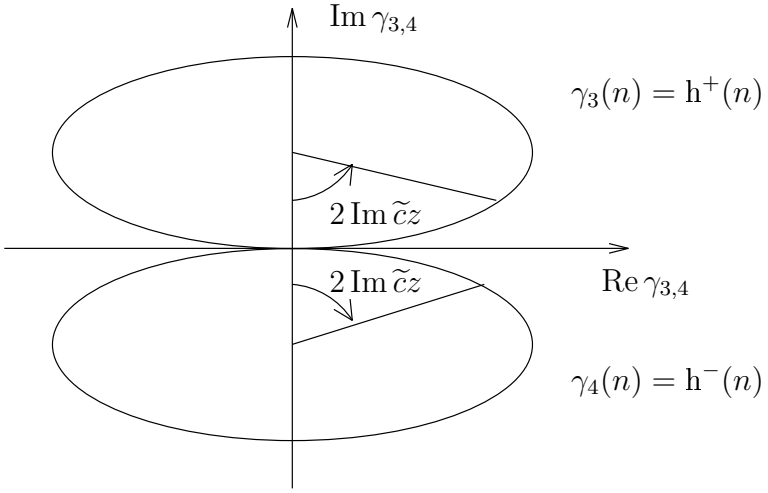

Figure 14: The eigenvalues $\gamma_{3,4}$ when $\widetilde{c}$ is imaginary. The major axes are $(2\,\mathrm{Im}\,\widetilde{c})^{-1}$ for both ellipses and the major- to minor-axis ratio is 2.

From (D.2) and (D.3) $\mathbf{M}(I)$, $\mathbf{N}(I)$ and $\mathbf{g}(I,J)$ can be calculated recursively for increasing I. From the start values, (D.3), $\mathbf{N}^L(0)$ and $\overrightarrow{\mathbf{g}}_L^-(0,J)$ are obtained. At $I = N-1$

$$\begin{pmatrix} \mathbf{M}_{11}^L(N-1) & \mathbf{M}_{21}^L(N-1) \\ \mathbf{N}_{11}^L(N-1) & \mathbf{N}_{21}^L(N-1) \end{pmatrix} = \sum_{i=0}^{N-2} \mathbf{Z}^i \begin{pmatrix} \mathbf{a} & \mathbf{b} \\ \mathbf{c} & \mathbf{d} \end{pmatrix} \begin{pmatrix} \mathbf{P}_\alpha^\tau(N-1-i) & \mathbf{0} \\ \mathbf{0} & \mathbf{P}_\beta^\tau(N-1-i) \end{pmatrix} + \mathbf{Z}^{N-1} \begin{pmatrix} \mathbf{0} & \mathbf{0} \\ \mathbf{0} & \boldsymbol{\delta}\mathbf{P}_\beta^\tau(0) \end{pmatrix},$$

$$\begin{pmatrix} \mathbf{M}_{12}^L(N-1) & \mathbf{M}_{22}^L(N-1) \\ \mathbf{N}_{12}^L(N-1) & \mathbf{N}_{22}^L(N-1) \end{pmatrix} = f(\mathbf{Z}) \begin{pmatrix} \mathbf{a} & \mathbf{b} \\ \mathbf{c} & \mathbf{d} \end{pmatrix} \begin{pmatrix} \mathbf{P}_\alpha^\rho & \mathbf{0} \\ \mathbf{0} & \mathbf{P}_\beta^\rho \end{pmatrix} + \mathbf{Z}^{N-1} \begin{pmatrix} \mathbf{0} & \mathbf{0} \\ \mathbf{0} & \boldsymbol{\delta}\mathbf{P}_\beta^\rho \end{pmatrix},$$

$$\begin{pmatrix} \overrightarrow{\mathbf{g}}_L^+(N-1,J) \\ \overrightarrow{\mathbf{g}}_L^-(N-1,J) \end{pmatrix} = \sum_{i=0}^{N-2} \mathbf{Z}^i \begin{pmatrix} \mathbf{a} & \mathbf{b} \\ \mathbf{c} & \mathbf{d} \end{pmatrix} \begin{pmatrix} \overrightarrow{\Sigma}_L^+(N-1-i,J) \\ \overrightarrow{\Sigma}_L^-(N-1-i,J) \end{pmatrix} + \mathbf{Z}^{N-1} \begin{pmatrix} \overrightarrow{0} \\ \boldsymbol{\delta}\overrightarrow{\Sigma}_L^-(0,J) \end{pmatrix}.$$

Here $f(x) = (1-x^{N-1})/(1-x)$ and $\mathbf{Z} = \begin{pmatrix} \mathbf{a}\mathbf{A}^\tau & \mathbf{a}\mathbf{A}^\rho \\ \mathbf{c}\mathbf{A}^\tau & \mathbf{c}\mathbf{A}^\rho \end{pmatrix}$. The last step gives

$$\begin{aligned}
\mathbf{M}_{11}^L(N) &= \boldsymbol{\alpha}\left[\mathbf{P}_\alpha^\tau(N) + \mathbf{A}^\tau\mathbf{M}_{11}^L(N-1) + \mathbf{A}^\rho\mathbf{N}_{11}^L(N-1)\right], \\
\mathbf{M}_{12}^L(N) &= \boldsymbol{\alpha}\left[\mathbf{P}_\alpha^\rho + \mathbf{A}^\tau\mathbf{M}_{12}^L(N-1) + \mathbf{A}^\rho\mathbf{N}_{12}^L(N-1)\right], \\
\mathbf{M}_{2k}^L(N) &= \boldsymbol{\alpha}\left[\mathbf{A}^\tau\mathbf{M}_{2k}^L(N-1) + \mathbf{A}^\rho\mathbf{N}_{2k}^L(N-1)\right], \\
\overrightarrow{\mathbf{g}}_L^+(N,J) &= \boldsymbol{\alpha}\left[\mathbf{A}^\tau\overrightarrow{\mathbf{g}}_L^+(N-1,J) + \mathbf{A}^\rho\overrightarrow{\mathbf{g}}_L^-(N-1,J) + \overrightarrow{\Sigma}_L^+(N,J)\right].
\end{aligned}$$

The above iteration give explicit, but perhaps not very useful, formulas for $\mathbf{M}$, $\mathbf{N}$ and $\mathbf{g}$. On the other hand, the domains of dependence are easily identified: $\mathbf{M}_{kl}^L(I)$ and $\mathbf{N}_{kl}^L(I)$ depend only on the initial values ($J = 0$) and $\mathbf{g}_L^\pm(I,J)$ depend only on the medium at previous times (time index $< J$). Hence, the notation in Eq. (4.2), with the built in domains of dependence, is justified.

Appendix Acknowledgements

The author would like to thank Prof. Gerhard Kristensson at the Department of Electromagnetic Theory at Lund Institute of Technology for enthusiasm and many interesting discussions during this project. Thanks also to Anders Karlsson and Sten Rikte for sharing their insights. Special thanks to Anders for the original algorithm. The work reported in this paper is supported by grants (TFR 91-849, 92-986 and 93-1145) from the Swedish Research Council for Engineering Sciences and their support is gratefully acknowledged.

References

[1] R. S. Beezley and R. J. Krueger. An electromagnetic inverse problem for dispersive media. *J. Math. Phys.*, **26**(2), 317–325, 1985.

[2] J. P. Corones, M. E. Davison, and R. J. Krueger. Direct and inverse scattering in the time domain via invariant imbedding equations. *J. Acoust. Soc. Am.*, **74**(5), 1535–1541, 1983.

[3] J. P. Corones and A. Karlsson. Transient direct and inverse scattering for inhomogeneous viscoelastic media: obliquely incident SH mode. *Inverse Problems*, **4**, 643–660, 1988.

[4] J. Fridén. Inverse scattering for anisotropic mirror image symmetric media. *Inverse Problems*, **10**(5), 1133–1144, 1994.

[5] J. Fridén, G. Kristensson, and R. D. Stewart. Transient electromagnetic wave propagation in anisotropic dispersive media. *J. Opt. Soc. Am. A*, **10**(12), 2618–2627, 1993.

[6] H. Goldstein. *Classical Mechanics.* Addison-Wesley, Reading, MA, USA, second edition, 1980.

[7] M. Hausner and J. T. Schwartz. *Lie Groups Lie algebras.* Thomas Nelson and Sons Ltd., London, 1968.

[8] A. Karlsson and G. Kristensson. Constitutive relations, dissipation and reciprocity for the Maxwell equations in the time domain. *J. Electro. Waves Applic.*, **6**(5/6), 537–551, 1992.

[9] G. Kristensson. Direct and inverse scattering problems in dispersive media—Green's functions and invariant imbedding techniques. In R. Kleinman, R. Kress, and E. Martensen, editors, *Direct and Inverse Boundary Value Problems*, Methoden und Verfahren der Mathematischen Physik, Band 37, pages 105–119, Frankfurt am Main, 1991. Peter Lang.

[10] G. Kristensson and S. Rikte. The inverse scattering problem for a homogeneous bi-isotropic slab using transient data. In L. Päivärinta and E. Somersalo, editors, *Inverse Problems in Mathematical Physics*, pages 112–125. Springer-Verlag, Berlin, 1993.

[11] G. Kristensson and S. Rikte. Transient wave propagation in reciprocal bi-isotropic media at oblique incidence. *J. Math. Phys.*, **34**(4), 1339–1359, 1993.

[12] I. V. Lindell. *Methods for Electromagnetic Field Analysis.* Clarendon Press, Oxford, 1992.

[13] J. M. Ortega. *Matrix Theory (A Second Course).* Plenum Press, New York, 1987.

[14] H. Otterheim. An inverse scattering problem for gyrotropic media. Technical Report TRITA-TET 93-3, Department of Electromagnetic Theory, S-100 44 Stockholm, Sweden, 1993.

[15] R. D. Stewart. *Transient electromagnetic scattering on anisotropic media.* PhD thesis, Iowa State University, Ames, Iowa, 1989.

[16] V. H. Weston. Time-domain wave-splitting of Maxwell's equations. *J. Math. Phys.*, **34**(4), 1370–1392, 1993.